9-5-2014

Structural and Functional Studies of GDP-6-Deoxy-Talose and GDP-Rhamnose Biosynthetic Enzymes

Benjamin E. Nicholson
Grand Valley State University

Paul D. Cook
Grand Valley State University

Structural and functional studies of GDP-6-deoxy-talose and GDP-rhamnose biosynthetic enzymes.

Ott-Steiner Endowed Fellowship of Natural Sciences of the S^3 Grant at Grand Valley State University.

Benjamin E. Nicholson, and Paul D. Cook PhD.

Office of Undergraduate Research, Department of Chemistry at GVSU.

September 5, 2014

Abstract:

GDP-6-deoxy-D-talose and its 4-epimer GDP-D-rhamnose are unusual sugars found on the cell surface of certain Gram-negative bacteria. GDP-6-deoxy-talose and GDP-rhamnose are produced by enzymes called GTS and RMD, respectively. These sugars are produced from the same common intermediate and are 4'-epimers of each other, which provides an interesting paradigm to study the stereo-selective reduction of unusual sugars. We have determined a novel X-ray crystallographic structure of RMD from *Pseudomonas aeruginosa* that contains its cosubstrate NADPH within the active site. A superposition of our RMD structure with a previously-determined one gives clear insight into the mechanism of hydride transfer from the cofactor during catalysis. We also report progress toward the structural analysis of GTS and functional analyses of both enzymes. Characterization of GTS and RMD will allow for an understanding of how bacteria utilize these sugars and may give insight into the pathogenicity of certain Gram-negative bacteria. Furthermore, an understanding of the production of unusual sugars can allow for the derivitization of existing antibiotics in an effort to combat bacterial resistance via a process called glycodiversification.

Introduction

Gram-negative bacteria contain a cell wall with an exterior structure called a lipopolysaccharide (LPS). The LPS plays an important role for the bacteria by signaling its identity to neighboring cells and plays a major role in the pathogenicity of the bacteria. The LPS contains a structure at its end called the O-antigen, which is comprised of sugars and differs from strain to strain in bacteria[1]. *Aggregatibacter*

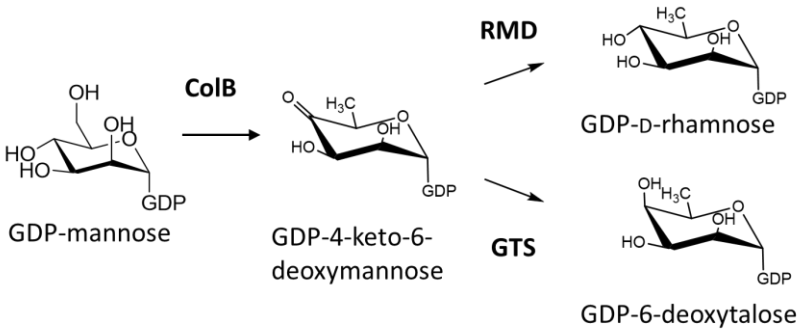

Scheme 1: Production of unusual sugars. This pathway shows the reduction of the common intermediate GDP-4-keto-6-deoxymannose into different unusual sugars. GDP-D-rhamnose and GDP-6-deoxytalose are 4-epimers of each other, indicating that RMD and GTS likely present a hydride to the 4 carbonyl of GDP-4-keto-6-deoxymannose from opposite faces.

actinomycetomcomitans is a pathogenic Gram-negative bacterial strain that causes gingivitis in children, and contains an extremely unusual sugar called GDP-6-deoxy-d-talose, which has only been found in one other bacteria strain. In studying the function of GDP-6-deoxy-d-talose, insights can be made to the pathogenicity of *A. actinomycetomcomitans*[2]. The epimer of GDP-6-deoxy-talose is GDP-d-rhamnose, which is a hexose sugar that differs from 6-deoxy-talose by only the orientation of the hydroxyl group on the C-4 position. GDP-d-rhamnose is natively found in the O-antigen of *Pseudomonas aeruginosa.* The synthetic pathway for both of these sugars is very similar, yielding a keto-sugar intermediate called GDP-4-keto-6-deoxy-d-mannose from a precursor GDP-d-mannose using the enzyme GDP-mannose-4,6-dehydratase (ColB)[3]. The production of GDP-d-rhamnose is catalyzed by the enzyme GDP-4-keto-6-deoxy-d-mannose-4-reductase (RMD) which utilizes a co-substrate NADPH for the addition of a hydride to the carbonyl of the sugar[4]. Detailed studies of the structure and function of RMD isolated from *Aneurinibacillus thermoaerophilus* were performed, and the enzyme's proposed catalytic activity has been characterized[3]. Four site-directed mutagenesis events were performed to determine function. The

133-threonine has been suggested to substitute the serine in the serine-tyrosine-lysine catalytic triad common to the SDR enzyme family. The Glu-135 was found to act as an active site general base[5]. The production of GDP-6-deoxy-d-talose has been proposed to be very similar to the production of GDP-d-rhamnose, with the addition of the hydride from NADPH proposed to add from the opposite face of the molecule. GDP-6-deoxy-d-talose synthase (GTS) catalyzes this reaction and utilizes the same co-substrate NADPH. Introductory functional studies have been performed on GTS, however, more steady-state kinetic and structural studies must be performed in order to completely understand the structure and function of GTS.

Antibiotic resistance has become a major issue in medicine in which bacteria produce enzymes that will render antibiotics inert. Some naturally-occurring antibiotic compounds contain unusual sugars and can be altered in order to change the structure of the antibiotic in a process called glycodiversification[4]. The replacement of an unusual sugar for the naturally-occurring sugar in an antibiotic may cause the antibiotic resistance enzyme to not be able to perform its function. By studying new unusual sugars, the library of sugars available for glycodiversification can be expanded and therefore used for drug design in combatting antibiotic resistant bacteria[5].

Experimental Procedures (Materials and Methods)

Expression and purification of GTS

Chemically competent *E. coli* (Rosetta strain) was transformed with pPDC053, a pET28 vector containing the TLD gene coding for GTS. The transformed cells were selected using 25 µg/mL of each chloramphenicol and kanamycin. The transformed cells were then surveyed for optimal growth conditions in LB and TB (terrific broth) cultures and allowed to grow to an optical density of 0.6 for LB and 0.8 for TB at 600 nm. IPTG was then added (1mM and 0.05mM for LB cultures and 0.1mM for LB cultures) and the cultures were shook for 20 hours at 200 rpm at 18˚C. The cells were the harvested by

centrifugation and the pellet was frozen at -20˚C. The cells were resuspended and lysed open using sonication. Purification was the preformed using nickel affinity chromatography. SDS-PAGE analysis was then used to determine presence and purify of GTS.

Kinetic Analysis:

A solution of 4-keto-6-deoxytalose was produced by using 0.05 mM $NAPD^+$, 1.6 mM GDP-mannose, 0.75 mg/mL of ColB. The reaction was carried out in a buffer containing 20 mM HEPES, 50 mM NaCl, and 5 mM $MgCl_2$ at pH 7.5 and was allowed to come to completion over the course of 15 hours. The reaction was centrifuged with an Amicon Ultra 10,000 kDal centrifugal filter to eliminate ColB for 20 min at 4000 rpm at 4˚C. The keto-sugar intermediate was then added to GTS at varying concentrations with 0.5 mM NADPH and the absorbance was measured at 340 nm using a Cary 60 UV-Visible spectrophotometer.

Analysis of Mutants:

Site-directed mutagenesis was performed to produce GTS Y128F. 10ng of pPDC053, 125 ng of each primer (oPDC117 and oPDC118), 5 µL of 10x pFu buffer, 3 µL of DMSO, and 1 µL of pFu ultra polymerase in 18 $M\Omega$ water to make a 50 µL reaction. The reaction was placed in a thermocycler. The mutagenesis program was set to be 95˚C for 1 minute, then cycle through 95˚C for 50 seconds, 50˚C for 50 seconds, and then 68˚C for 13 minutes, and it was repeated 20 times. The program was then set to hold for 7 minutes at 68˚C and then hold at 4˚C. After being removed from the thermocycler, 1 µL of Dnp1, I µL of DNA Ligase, and Ligase buffer was added to the mutagenesis reaction and the reaction was allowed to sit for 3 hours. The reaction was the transformed into XL1-Blue *E. coli* cells.

Recombination of TLD into pTyb12:

A restriction digest reaction was mixed and incubated overnight at 37˚C. The reaction contained 2.5% Nde1 and Xho1, 50% DNA, and CutSmart buffer. One reaction contained pPDC053 and the other contained pTyb12. The restriction digest reactions then underwent gel electrophoresis using 1% agarose gel with ethidium bromide as the DNA dye. The DNA was then extracted using a Thermo Scientific gel extraction kit. The pTyb12 vector and the TLD gene were then ligated together, using 50 ng of each DNA sample with 10% ligase in ligase buffer. The reaction was incubated for 5 hours at 16˚C, and then the ligated DNA was transformed into XL1-Blue cells and selected using ampicillin (25 µg/mL). Successful recombination was verified by preforming a restriction digest of the miniprepped ligation product. Nde1, Xho1, and the plasmid vectors were all missed with CutSmart buffer and incubated at 37 ˚C for 2 hours. The reactions were tested using gel electrophoresis.

Expression and Purification of GTS:

Chemically competent *E. coli* (BL-21) was transformed with pPDC053, a pET28 vector containing the TLD gene coding for GTS. The transformed cells were selected using 25 µg/mL of kanamycin. The transformed cells were then allowed to grow to an optical density of 0.8 at 600 nm in TB. IPTG was then added (0.1mM) and the cultures were shook for 20 hours at 200 rpm at 18˚C. The cells were the harvested by centrifugation and the pellet was frozen at -20˚C. The cells were resuspended and lysed open using sonication. Purification was the preformed using nickel affinity chromatography with fractional collection. SDS-PAGE analysis was then used to determine presence and purify of GTS. The histidine nucleotide tag was cleaved using TEV-cleavage. The reaction was incubated for 12 hours at 25 ˚C. SDS-PAGE analysis was utilized again to determine presence and purity of GTS. A second method was used to attempt to purify GTS. BL-21 cells were transformed with pPDC054, a pTyb12 vector containing TLD. An expression survey was performed in the same fashion as previously

stated. Purification was performed using chitin affinity chromatography, using the IMPACT purification system. Purification efficiency was tested using SDS-PAGE. The chitin affinity chromatography method was attempted a second time, using Rosetta cells to express GTS. GTS Y128F was also expressed an purified using BL21 cells and nickel affinity chromatography with all solutions containing 10% glycerol.

Expression and Purification of RMD and ColB:

BL-21 cells were transformed with pPDC052 and pPDC007, pET28 vectors containing the gene coding for RMD for *Pseudomonas aeruginosa* and the gene coding for ColB, a 4,6-dehydrotase that produces 4-keto-6-deoxytalose. Expression was performed as previously stated and purification was performed using nickel-affinity chromatography. Purification validation was obtained using SDS-PAGE.

Crystallization Trials of RMD and GTS Y128F:

RMD and GTS Y128F crystallization trials were attempted using the hanging drop diffusion method. RMD crystallization trials were attempted in its apoenzyme form, and with 5 mM NADPH. Potential crystals were frozen in liquid nitrogen using 20% ethylene glycol. The crystals were then tested using X-ray crystallography at the Argonne National Laboratory's Advanced Photon Source. Useable data was collected for RMD bound to NADPH and in its apoenzyme form. The RMD structure with NADPH bound was solved.

Results

Expression and purification of GTS, RMD and ColB:

SDS-PAGE analysis in Figure 1 shows no appreciable pure GTS in any of the conditions tested. All attempts to purify GTS showed impure samples and too little of GTS purified (Figures 2-4).

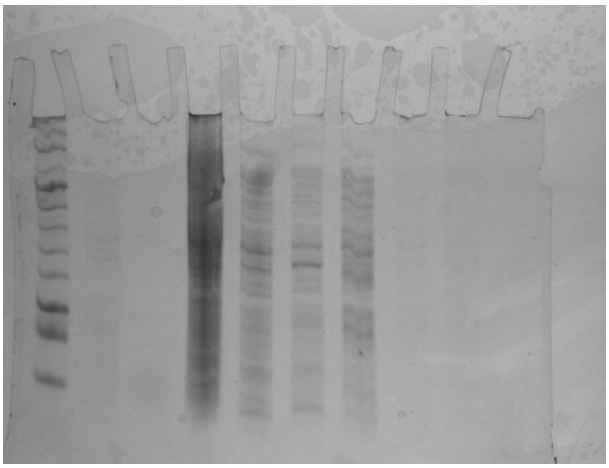

Figure 1: SDS-PAGE gel showing expression of GTS in Rosetta cells: The gel above shows protein expression of GTS for the different media conditions of Rosetta cells. Lane 1 shows a protein ladder. Lanes 2, 3 and 4 show cell lysate samples of TB, LB with 1 mM IPTG and LB with 0.05 mM IPTG respectively. Lanes 5, 6 and 7 show pure GTS samples of TB, LB with 1 mM IPTG and LB with 0.05 mM IPTG respectively.

Figure 2: SDS-PAGE analysis of purification of GTS through fractional collection. The above gel shows SDS-PAGE results of GTS purification via fractional collection. Lane one contains a protein ladder, lane two contains a clarified lysate sample, and lanes 3-8 contain fractions. The band consistent through all lanes is speculated to be a result of using homemade running buffer. No fractions appeared to contain any viable protein.

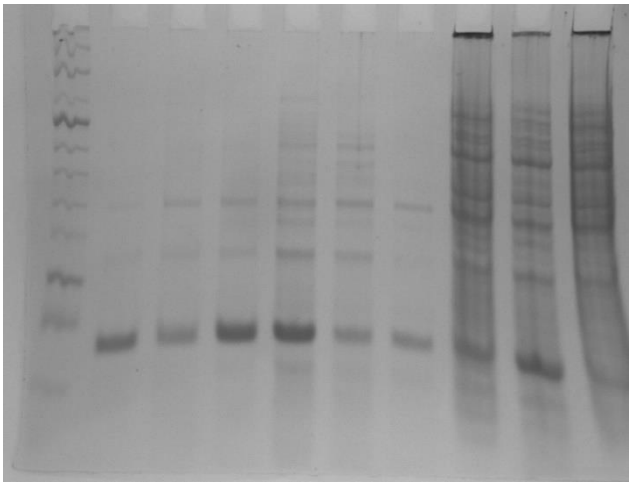

Figure 3: SDS-PAGE of chitin binding survey. This gel shows the results from SDS-PAGE of samples from the chitin binding expression survey. Lane 1 is a protein ladder. Lanes 2, 3 and 4 are the chitin resin samples of LB with 0.05 mM IPTG, LB 1 mM IPTG and TB samples respectively. Lanes 5, 6 and 7 are clarified lysates of LB with 0.05 mM IPTG, LB 1 mM IPTG and TB samples respectively. Lanes 8, 9 and 10 are whole cell lysates of LB with 0.05 mM IPTG, LB 1 mM IPTG and TB samples respectively. The chitin resins showed a significant peak at around 100,000 kDal.

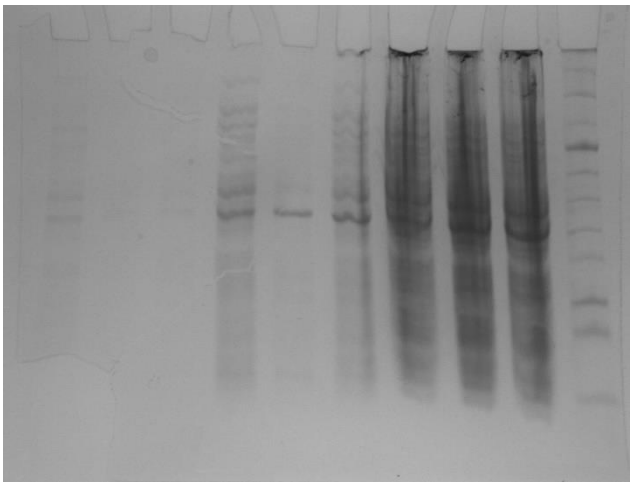

Figure 4: SDS-PAGE analysis of GTS purification in Rosetta cells. The gel above shows the SDS-PAGE results of the expression of GTS in the pTyb12 vector in Rosetta cells. Lane 1, 2 and 3 contain pure GTS samples of TB, LB with 0.05 mM IPTG and LB 1 mM IPTG samples respectively. Lane 4, 5 and 6 contain clarified lysates samples of TB, LB with 0.05 mM IPTG and LB 1 mM IPTG samples respectively. Lanes 7, 8 and 9 contain whole cell lysate samples of TB, LB with 0.05 mM IPTG and LB 1 mM IPTG samples respectively. Lane 10 contains a protein ladder. Prominent band throughout samples resides at 50,000 kDal.

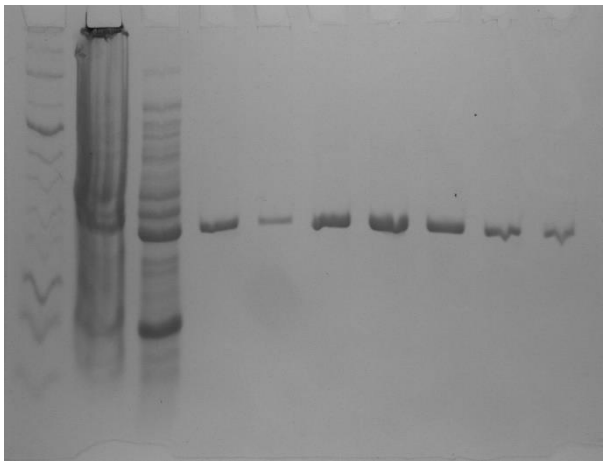

Figure 5: SDS-PAGE of RMD purification. The gel above shows purification of RMD through nickel affinity chromatography through fractional collection. Lanes 1 through 7 contains separate fractions, lane 8 contains clarified lysate, lane 9 contains whole cell lysate, and lane 10 contains a protein ladder.

RMD and ColB both showed pure bands throughout fractions or elution steps (Figure 5,6). The attempt to purify GTS Y128F with 10% glycerol in purification step solutions showed a significant more amount of GTS, but, a larger protein was unable to be purified from GTS (Figure 7).

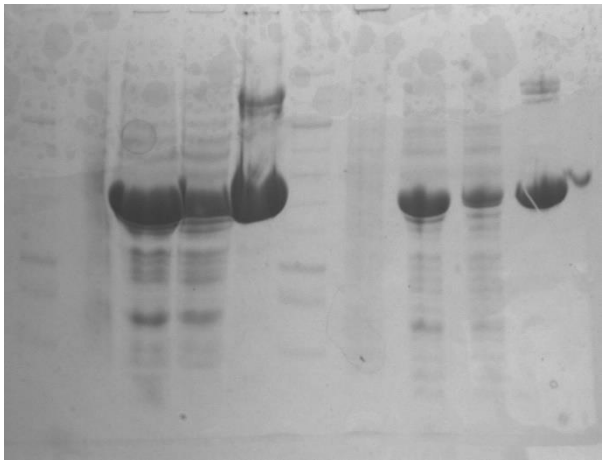

Figure 6: SDS-PAGE of ColB purification. The gel shows purification of ColB with nickel affinity chromatography. Lanes 1 and 6 show protein ladders, lanes 2 and 6 show whole cell lysates, lanes 3 and 7 show clarified lysates, lanes 4 and 9 show flow-through samples and lanes 5 and 10 show purified ColB samples. The 5 lanes on the right were diluted on the left for a higher resolution.

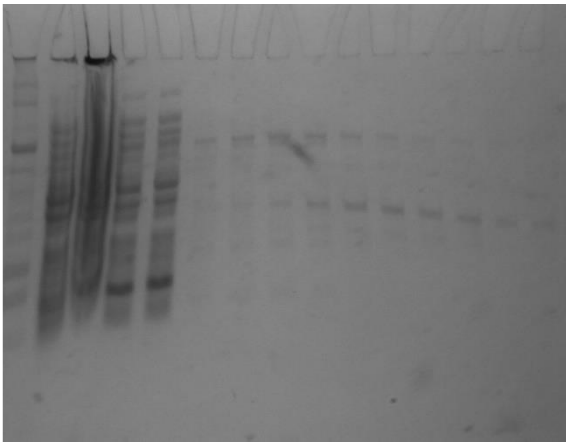

Figure 7: SDS-PAGE analysis of GTS mutant Y128F purification. The gel above shows fractional collection nickel affinity chromatography purification of GTS Y128F mutant. Lanes 1-10 contain fractions collected, lane 11 contains flow through, lane 12 contains the clarified lysate, lane 13 contains a whole cell lysate, lane 14 contains a pre-induction sample and lane 15 contains a protein ladder. Fractions from lanes 1 to 7 were collected. Lanes 1 through 9 show a band a 33,000 kDal corresponding with the GTS mutant. A contaminant is present in fractions in lanes 3 through 10.

Kinetic Analysis:

Preliminary GTS activity assay in Figure 4 showed a linear relationship with different volumes of GTS added. The R^2 value was found to be 0.95.

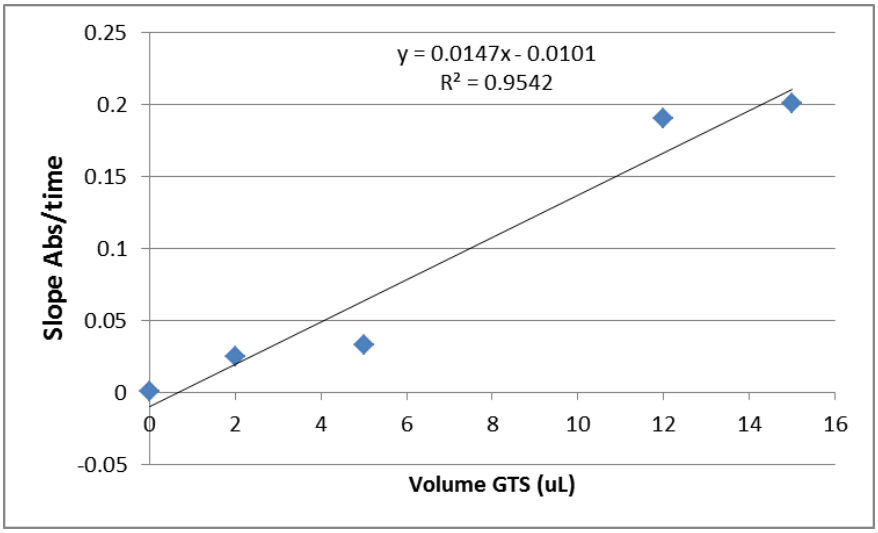

Figure 8: Activity plot of GTS. The plot above shows activity of GTS with different volumes of GTS (impure sample). The relationship was linear, however, only has an R^2 value of 0.95.

Analysis of Mutants:

A sequence alignment of the site-directed mutagenesis of GTS Y128F compared the wildtype determined the successful single mutation of GTS at the 128 position.

Recombination of TLD into pTyb12:

Two of the four tested plasmids contained the TLD gene as shown in Figure 5. This is supported by the fact that both lanes contain a band corresponding with 6000 base pairs and a band corresponding with 900 base pairs. The other two lanes do not contain TLD since they do not have a corresponding band for TLD.

Crystallization Trials of RMD and GTS Y128F:

A data set was collected for RMD in conditions containing 200 mM lithium nitrate with 20% PEG 3350 and 5 mM NADPH. The structure was solved to a max resolution of 1.91 Angstroms. The asymmetric unit was found to contain four monomers. Table 1 shows crystallization statistics from the data collection and refinement process.

The structure was found to show an interaction between the biological dimer at a four-helical bundle (Figure 9). The NADPH was found to be well ordered throughout the active site. The NADPH model in Figure 10 fits the F_0-F_{20} map from our RMD crystallographic data very well. This result supports the orientation of the NADPH molecule within the active site. A superposition of the previous structure of RMD from *Aneurinibacillius* with our recently solved structure shows a strong correlation between characteristics of the enzyme from both bacterial strains. The superposition shows similar direction and position of the majority of NADPH, TYR-130, and the alpha trace around the active site. The enlarged active site superposition shows the orientation that the nicotinamide ring is in relation to the sugar analog.

Data collection statistics	
Resolution (Å)	34.03-1.91 (1.94-1.91)
Completeness (%)	99.1 (98.5)
Avg *I* / Avg $\sigma(I)$	8.5 (1.6)
R_{merge} (%)	9.0 (68.1)
Refinement statistics	
$R_{overall}/R_{free}$ (%)	19.2/23.5
RMSD bond lengths (Å)	0.023
RMSD bond angles (°)	1.9
Average protein B values (Å^2)	34.8
Average solvent B values (Å^2)	33.9
Average ligand B values (Å^2)	28.7

Note: values in parentheses are for the highest resolution bin

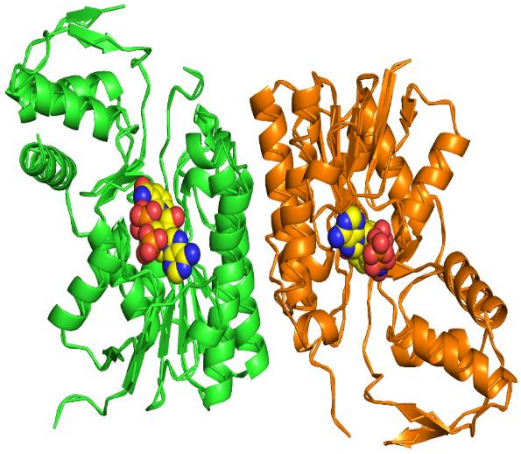

Figure 9: Structure of RMD WT with bound NADPH. This structure shows the biological unit of RMD as determined X-

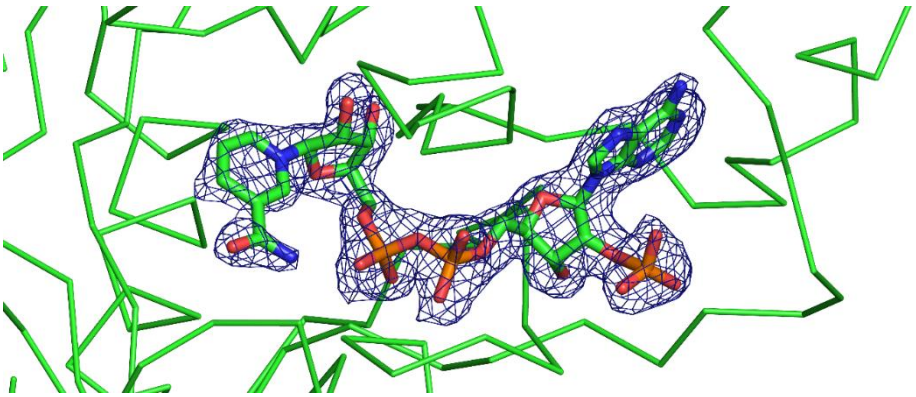

Figure 10: X-ray crystallographic data fitting NADPH model in RMD active site. The above NADPH model is fit to F_0-F_{20} map from our RMD crystallographic data. The model shows a well ordered NADPH, with a 1.9 resolution map. The background ribbon is the alpha carbon trace of the enzyme. On the right is the adenine nucleotide with a diphosphate bridge in the middle connecting the nicotinamide ring on the left.

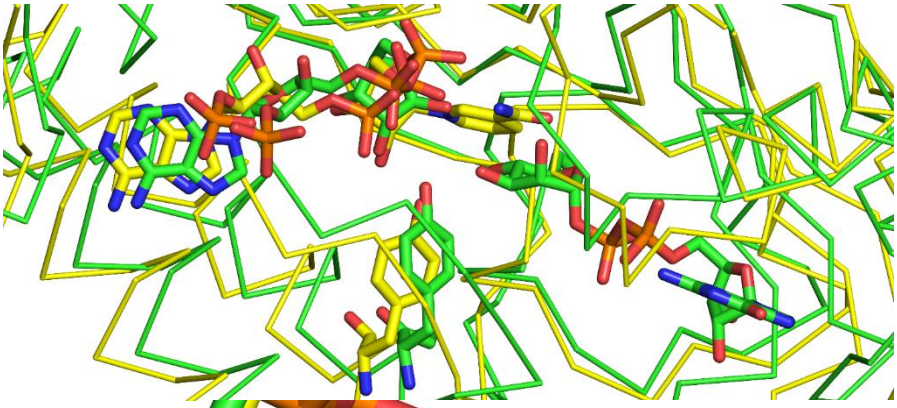

Figure 11: Active site superposition of previously determined RMD structure with newly determined structure. This figure shows an overlay of the active site of RMD. Green traces correspond with the previously determined structure, which contains an NADPH analog missing the nicotinamide ring, and GDP-mannose, a sugar analog to 6-deoxy-4-keto-GDP-mannose. The green structure was obtained from *Aneurinibacillius.* The yellow trace corresponds with the newly determined structure containing NADPH.

Discussion

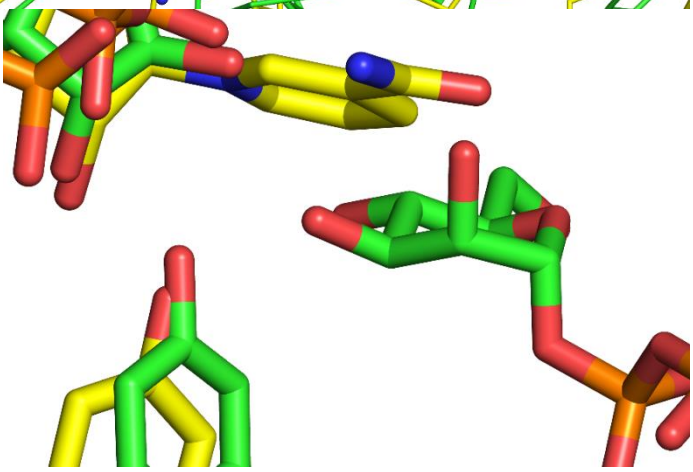

Figure 12 enlarged superposition of RMD structures. This figure shows an enlarged version accentuating a potential interaction between NADPH and the sugar. This structure shows a bound GDP-mannose, an analog of 6-deoxy-4-keto-GDP-mannose.

Methods attempted for the purification of GTS have so far been unsuccessful for quantities necessary for functional and structural studies. More methods of purifications are currently being pursued. Kinetic analysis of GTS showed a linear relationship with the addition of more enzyme. This shows that the only enzyme acting on the substrate is GTS, and therefore more kinetic analysis can be performed under these circumstances. The sequence alignment of GTS Y128F showed that a successful mutation of the 128-Tyr residue was accomplished. Kinetic and crystallographic analysis can now be performed on GTS Y128F to determine the catalytic role of 128-Tyr in the function of GTS.

The crystallization statistics of RMD show that the data was able to be solved with reliable certainty. Refinement statistics show that the model was fit the data with reasonable certainty and reliability. Figure 10 shows the well-ordered NADH within the active site, and supports the positioning within the active site of RMD. The superposition of the two RMD structures in figures 11 and 12 leads to the conclusion that the hydride is donated from the particular side that leaves the 4’ carbon of 4-keto-6-

deoxytalose to be in the R orientation, leaving the resulting sugar to be rhamnose. The positioning of the hydride donation site of the nicotinamide in relation to the sugar analog supports this mechanism for hydride transfer. A sugar-bound structure with NADPH of RMD would further support the evidence leading towards this conclusion. The orientation and proximity of 131-Tyr supports previous postulates that the particular residue acts as a catalytic acid in the RMD reaction. Further structural and functional studies of RMD and GTS will allow for comparison of both reactions for a greater understanding of the production of unusual sugars.

Acknowledgments

We would like to thank Les and Jackie Steiner for graciously donating their funds to support the Ott-Steiner Fellowship of Natural Sciences for the Student Summer Scholars (S^3) program at GVSU. We would also like to thank the Department of chemistry for supporting out needs and supplying us with materials and equipment for use. We would like to thank the Office of Undergraduate Research at GVSU for organizing and making the S^3 program possible. We would also like to thank the Wheldon fund for providing preliminary funds for our laboratory. Jeanne Stoddard for the Medical Laboratory Sciences at GVSU is also greatly appreciated for graciously providing the *Aggregatibacter* culture.

References

1. Samuel, G. & Reeves, P. Biosynthesis of O-antigens: genes and pathways involved in nucleotide sugar precursor synthesis and O-antigen assembly. *Carbohydrate Research* **338,** 2503–2519 (2003).
2. Mäki, M. *et al.* Cloning and functional expression of a novel GDP-6-deoxy-D-talose synthetase from Actinobacillus actinomycetemcomitans. *Glycobiology* **13,** 295–303 (2003).
3. King, J. D. *et al.* The structural basis for catalytic function of GMD and RMD, two closely related enzymes from the GDP-d-rhamnose biosynthesis pathway. *FEBS Journal* **276,** 2686–2700 (2009).
4. Somoza, J. R. *et al.* Structural and kinetic analysis of Escherichia coli GDP-mannose 4,6 dehydratase provides insights into the enzyme's catalytic mechanism and regulation by GDP-fucose. *Structure* **8,** 123–135 (2000).
5. Zhang, C. *et al.* Exploiting the reversibility of natural product glycosyltransferase-catalyzed reactions. *Science* **313,** 1291–1294 (2006).